A novel human iPSC model of COL4A1/A2 small vessel disease unveils a key pathogenic role of matrix metalloproteinases

A novel human iPSC model of COL4A1/A2 small vessel disease unveils a key pathogenic role of matrix metalloproteinases

Authorship:

Maha Al-Thani*[1], Mary Goodwin-Trotman*[1], Steven Bell[1], Krushangi Patel[1], Lauren K Fleming[2], Catheline Vilain[3], Marc Abramowicz[3], Stuart M Allan[4,5], Tao Wang[5], Zameel Cader[6], Karen Horsburgh[7], Tom Van Agtmael[2], Sanjay Sinha[10], Hugh S Markus[9], and Alessandra Granata[1].

Affiliation

1 Department of Clinical Neurosciences Department, Heart and Lung Research Institute, University of Cambridge and Royal Papworth Hospital, Cambridge, UK
2 School of Cardiovascular and Metabolic Health, University of Glasgow, Glasgow, UK
3 Department of Genetics, Hôpital Erasme, ULB Center of Human Genetics, Universite Libre de Bruxelles, Bruxelles, Belgium
4 Lydia Becker Institute of Immunology and Inflammation, Division of Neuroscience and Experimental Psychology, School of Biological Sciences, Faculty of Biology, Medicine and Health, The University of Manchester, Manchester Academic Health Science Centre, Manchester, UK
5 Geoffrey Jefferson Brain Research Centre, Manchester Academic Health Science Centre, Northern Care Alliance NHS Foundation Trust, University of Manchester, Manchester, UK
6 School of Biological Sciences, Translational Molecular Neuroscience Group, Weatherall Institute of Molecular Medicine, Nuffield Department of Clinical Neurosciences, University of Oxford, Oxford, UK
7 Centre for Discovery Brain Sciences, University of Edinburgh, Edinburgh, UK
8 Wellcome-MRC Cambridge Stem Cell Institute, Jeffrey Cheah Biomedical Centre, University of Cambridge, UK
9 Department of Neurology, Cambridge University Hospitals NHS Foundation Trust, Cambridge, UK

*co-first author
† Correspondence to ag686@cam.ac.uk

Summary

Cerebral small vessel disease (SVD) affects the small vessels in the brain and is a leading cause of stroke and dementia. Emerging evidence supports a role of the extracellular matrix (ECM), at the interface between blood and brain, in the progression of SVD pathology but this remains poorly characterized.

To address ECM role in SVD, we developed a co-culture model of mural and endothelial cells using human induced pluripotent stem cells from patients with *COL4A1*/*A2* SVD-related mutations. This model revealed that these mutations induce apoptosis, migration defects, ECM remodelling and transcriptome changes in mural cells. Importantly, these mural cell defects exert a detrimental effect on endothelial cells tight junctions through paracrine actions. *COL4A1/A2* models also express high levels of matrix metalloproteinases (MMP) and inhibiting MMP activity partially rescues the ECM abnormalities and mural cell phenotypic changes. These data provide a basis for targeting MMP as a therapeutic opportunity in SVD.

Introduction

Cerebral small vessel disease (SVD) is a leading cause of age-related cognitive decline and contributes to up to 45% of dementia cases worldwide (Gorelick et al., 2011). SVD is also responsible for 20% of ischemic strokes and is a common pathology underlying intracerebral haemorrhages (ICH) (Wardlaw et al., 2019). SVD refers to the sum of all pathological processes that affect the small vessels of the brain and with an aging population, SVD has major and growing global socio-economic impact (Lam et al., 2022). However, despite its importance, therapeutic approaches for SVD remain limited due to the lack of mechanistic understanding and relevant models required for target identification and drug discovery (Smith and Markus, 2020).

SVD features are associated with advancing age and several vascular risk factors (Wardlaw et al., 2014). Genetic factors have also been reported to be important with the identification of monogenic forms of SVD (Mancuso et al., 2020) and common variants which increase the risk of sporadic SVD (Chung et al., 2021.; Rannikmäe et al., 2015; Traylor et al., 2021). Dominant mutations in collagen type IV, a major component of the microvascular extracellular matrix (ECM), cause SVD presenting with both ICH and ischaemic (Gould et al., 2005; Jeanne et al., 2012). *COL4A1* and *COL4A2* mutations cause highly penetrant multi-system disorders, by disrupting the ECM homeostasis and leading to ICH and porencephaly in human and mouse models (van Agtmael et al., 2005; Joutel and Faraci, 2014; Murray et al., 2014). Most mutations occur in a glycine (G) residue of the G-X-Y repeat, that characterises the collagenous domain and the position of the mutation appeared to correlate with SVD severity (Jeanne et al., 2015). Conversely, variant within the 3′ untranslated region of *COL4A1* located in a putative miR-29 microRNA binding site results in *COL4A1* upregulation and causes a severe form of ischemic SVD, distinct from *COL4A1* missense glycine mutations phenotype (Siitonen et al., 2017; Verdura et al., 2016). Patients' fibroblasts with *COL4A1* and *COL4A2* gene duplications have also shown increased gene expression, supporting evidence for the pathogenicity of *COL4A1A/2* overexpression in SVD (Kuuluvainen et al., 2021). Importantly, both monogenic and sporadic forms of *COL4A*-related SVD are likely to share similar pathological mechanisms since rare coding variants in *COL4A1/A2* also occur in sporadic forms of ICH while common *COL4A1/A2* non-coding variants have been identified as risk factor for sporadic lacunar stroke (Chung et al., 2019; Persyn et al., 2020; Traylor et al., 2021), sporadic ICH (Malik et al., 2018; Rannikmäe et al., 2015) and white matter hyperintensities (Persyn et al., 2020) in the general population. This suggests that insights gained from a model of monogenic *COL4A1/A2* are likely to be relevant to common SVD. Although the mechanisms leading to SVD are ill-defined, there is an emerging focus on the role of the ECM. The ECM of cerebral blood vessels is a key component at the interface between the cerebral microcirculation and the brain, providing structural support to the blood brain barrier (BBB) as well as influencing cell behaviour (Joutel et al., 2016). Genetic studies have revealed that most monogenic forms of SVD are caused by mutations in genes either encoding ECM proteins, or in proteins regulating ECM function (Joutel et al., 2016). In addition to this, our recent work has found that genes related to SVD, including *COL4A1* and *COL4A2*, are significantly enriched in the cerebrovascular ECM network in both mouse and human brain (Pokhilko et al., 2021). To date, the mechanisms by which these ECM defects cause disease remains poorly understood. This underscores the clear need for new models relevant to human SVD.

To provide insights into the pathological mechanisms underlying COL4A1/A2-related SVD, we established a human induced pluripotent stem cells (hiPSC)-based 'disease in a dish' model from two individuals with two representative glycine substitutions in the G-X-Y repeat, one in *COL4A1* (G755R) and the other in *COL4A2 (G702D)* gene (Murray et al.,

2014; Shah et al., 2010). We differentiated the hiPSC into mural cells and endothelial cells and undertook phenotypic and functional assays and transcriptomic analysis.

Results

Establishment and characterisation of COL4A1/A2 hiPSC-derived mural cells and endothelial cells

Two hiPSC lines with typical SVD-associated SNPs in *COL4A* genes were used in this study: a *COL4A1*^{G755R} with a G>A substitution in exon 30 of *COL4A1* gene resulting in a change from a glycine to arginine at position 755 from a symptomatic patient and a *COL4A2*^{G702D} with a G>A replacement in exon 28 of *COL4A2* gene, resulting in a change from a glycine to aspartic acid at position 702 from the asymptomatic father of a patient (**Table S1)** (Murray et al., 2014; Shah et al., 2010). To control for genetic background, we generated isogenic corrected lines, in which the mutant allele (A) in *COL4A1* and *COL4A2* hiPSCs were substituted with the wild-type (WT) allele (G), two subclones were used for each CRISPRed line (**Table S1-2; Figure S1A**). As further controls, we used three wild-type (WTs) hiPSC lines from healthy individuals (**Table S1**). hiPSC lines were characterised for pluripotency markers expressions by immunostaining, qPCR profiling and formation of the 3-germ layers (**Figure S1B-D**). hiPSC were successfully differentiated into mural cells of neural crest origin (MC) as previously described (Cheung et al., 2012; Serrano et al., 2019) **(Figure S2A)** and characterised for specific markers expression for neural crest (**Figure S2B,C**) and for mural cells markers at day 12 of PDGFBB+TFG-β1 differentiation (PTD12) at mRNA levels (**Figure S2D**) and at fully differentiated stage at 2 weeks in serum containing media (2WS) by immunohistochemistry and qPCR (**Figure 1A,B; Figure S2D,E**).

MC express both specific markers for smooth muscle cells (*CNN1, ACTA2, TAGLN*) and pericytes (*NG2* and *PDGFRA*), with the disease lines showing significantly increased expression levels for *CNN1* and *ACTA2* at late stage of differentiation (2WS) (**Figure 1B; Figure S2D)**. MC are known to produce a variety of ECM proteins, including collagen IV. To assess collagen IV levels in the ECM, both *COL4A1/A2* disease and isogenic hiPSC-derived MC were plated at equal density, decellularized and stained with a specific antibody which recognised both collagen IV α1 and α2 chains (**Figure 1C**). There was a significant reduction in collagen IV staining in the ECM of the disease *COL4A1/A2* mutant lines compared to the controls, as seen in patient fibroblasts (**Figure 1D)** (Murray et al., 2014). Moreover, hiPSC-derived MC with *COL4A1*^{G755R} and *COL4A2*^{G702D} have increased migration ability in a scratch assay compared to controls (**Figure 1E,F).** MC 2WS also exhibit higher apoptotic levels, when stained for Annexin V and Propidium iodide (PI) by flow cytometry compared to the controls (**Figure 1G,H (b))**, similar to previous findings from primary patient fibroblasts and skin biopsy (Murray et al., 2014). Interestingly, no significant changes in apoptotic rates were seen at earlier stage (PTD12; **Figure 1G, H(a)**), at which stage ECM deposition of collagen IV cannot be detected (**Figure S2F,G**). Thus, higher apoptotic rates might be a consequence of increased levels of abnormal collagen IV in the ECM. These data indicate that our hiPSC-MC recapitulate defects of *COL4A1/2* mutations and thus represent a valid model to explore disease mechanisms.

Mural cells contribute to the barrier phenotype in a co-culture and paracrine systems

Brain endothelial cells are known for their barrier function in the BBB, which may be compromised in SVD pathology (Hussain et al., 2021). However, the impact of collagen IV mutations on the BBB and cross talk between endothelial cells and MC remains poorly understood. To assess this, *COL4A1/A2* disease, isogenic and WT lines were differentiated into brain microvascular endothelial-like cells (BMEC) using a previously established protocol (**Figure S3A;** (Hollmann et al., 2017)). These BMEC were

characterised for expression of specific markers by flow cytometry and qPCR (**Figure S3B-D).** BMEC were then plated onto a 2D transwell setting alone or in presence of MC plated on the basolateral side and maintained for 6 days (**Figure 2A)**. During this time, daily readings were taken of transendothelial electrical resistance (TEER), a robust indicator of endothelial cell barrier integrity. TEER measurement expressed as peak values relative to blank (transwell with no cells) for BMEC alone and in co-culture with MC were compared (**Figure 2B).** Isogenic and WT control MCappear to promote barrier function by significantly increasing TEER values, while disease MC have little effect on *COL4A1/A2* BMEC TEER (**Figure 2B).** Moreover, MC were culture with or without the addition of ascorbic acid in the media to promote collagen synthesis and similar results were obtained.

Since in this setting, there is no cell-cell interaction between MC and BMEC, we further assessed the differential MC paracrine effect on the barrier properties, by treating the isogenic BMEC clones with conditioned media of *COL4A1/A2* MC and vice versa for 6 days (**Figure 2C).** Interestingly, TEER values of disease BMEC tend to benefit from isogenic MC paracrine effect (**Figure 2D).** Conversely disease MC exert a paracrine effect by significantly decreasing TEER values in isogenic BMEC (**Figure 2E).** This MC mediated paracrine effect on barrier phenotype was confirmed by sodium fluorescein (NaF) size exclusion paracellular permeability assay (**Figure 2F)**, with the isogenic MC decreasing NaF permeability, thus promoting barrier tightness (**Figure 2G**), while disease MC appear to increase barrier permeability in isogenic BMEC (**Figure 2H)**. Collectively, these data show the secretome of disease MC to have detrimental effects on barrier function in *COL4A1/A2* SVD models.

COL4A1/A2 mural cells affect endothelial tight junction levels and distribution via a paracrine effect

The integrity of tight junctions is essential for the BBB properties of brain endothelial cells (Nitta et al., 2003; Pan et al., 2017). Thus, to assess if tight junctions are affected in *COL4A1/A2* hiPSC-derived BMEC, we performed immunostaining analysis for the tight junction proteins, occludin and claudin-5 (**Figure 3A**). We observed striking discontinuities in occludin staining (white arrow) and frayed junctions evident with claudin-5 staining (white arrowhead) in $COL4A1^{G755R}$ and $COL4A2^{G702D}$ BMEC cultured alone. These abnormalities were significantly more frequently in the mutant lines compared to controls (**Figure 3B)**. Moreover, this was associated with reduced occludin and claudin-5 total protein levels (**Figure 3C,D)**.

To independently validate these findings and exclude they were due to the differentiation protocol, we adopted an alternative endothelial differentiation protocol to generate hiPSC-derived EC (iECS; **Figure S3E)** (Orlova et al., 2014a, 2014b). These iECs were characterised for expression of specific markers at mRNA levels by qPCR compared to human umbilical vein endothelial cells (HUVEC) as positive control (**Figure S3F)** and flow cytometry (**Figure S3G**) and were found to have increased discontinued/frayed junctions as well as lower levels of occludin and claudin-5 proteins in disease lines versus controls (**Figure S4A-D**), validating our findings in BMEC.

To assess if the levels and the distribution of occludin and claudin-5 in endothelial cells is regulated by the MC secretome, $COL4A1^{G755R}$ and $COL4A2^{G702D}$ hiPSC-BMEC were treated with isogenic MC conditioned media for 4 days prior to immunostaining (**Figure 3E**). Notably, treatment with isogenic MC media significantly improved the presence of discontinuous and frayed junctions (**Figure 3F**). Conversely, a greater number of discontinuous and frayed junctions was observed when both isogenic BMEC clones were treated with conditioned media from mutant *COL4A1/A2* MC (**Figure 3G,H).** These data

clearly support that COL4 SVD includes tight junction defects in endothelial cells that are determined at least in part by a paracrine effect exerted by the MC.

Transcriptomic analysis highlights ECM abnormalities in COL4A1/A2 mural cell lines

To identify potential mediators of the MC paracrine effects reported above, we performed a transcriptomic analysis on *COL4A1*^{G755R} and *COL4A2*^{G702D} and corresponding isogenic hiPSC-MC in culture in serum containing media for a week (**Figure 4A**). From the bulk RNA sequencing data, we identified 374 differentially expressed genes (DEGs). No significant difference was observed for COL4A1 and A2 mRNA levels between disease and control lines. Importantly, it emerged that 56 DEGs were ECM proteins, and that matrix metalloproteinase (MMPs) were among the proteins misregulated (**Figure 4B; Table S5 and S6**). It is known that changes in MMPs levels are associated with barrier disruption and stroke (Candelario-Jalil et al., 2011; Clark et al., 1997; Wallin et al., 2017). To validate the transcriptomics findings, we perform qPCR in early MC (PTD12) and late MC (2WS) to profile MMP gene expression (**Figure 4C,D**). We observed a biphasic expression for *MMP2*, which appears to be downregulated at PTD12 and upregulated at late stage (MC 2WS). *MMP9* mRNA levels were also found to be upregulated in both *COL4A1* and *A2* MC at late stage (**Figure 4D).** *MMP7* shows high expression levels at PTD12 (**Figure 4C)**. In addition, we also found a significant increase in *MMP14* mRNA levels in *COL4A1/A2* BMEC (**Figure 4E**). Interestingly, MMP14 which activates pro-MMP2, was also previously reported to be upregulated in aorta of mice with a *Col4a1* glycine mutation (*Col4a1*$^{+/SVC}$ G1064D) that is a well-established model of Col4a1 associated SVD (**Figure S5A,B)** (van Agtmael et al., 2005; Jones et al., 2016, 2019)**.** The *MMP14* increase was also validated at protein levels in *COL4A1/A2* BMEC and iECs (**Figure S5C,D).** These data clearly support that the ECM and MMPs are dysregulated in *COL4A1/A2* MC.

MMP inhibition rescues phenotypic alterations, ECM and tight junction defects.

Since, MMPs are important for matrix remodelling, including collagens, and because they also target tight junctions for degradation, we hypothesized that MMPs could mediate the *COL4A1/A2* ECM phenotype seen in our *in vitro* model. Thus, we proceeded to treat *COL4A1/A2* hiPSC-derived BMEC with the pan-MMPs inhibitor, doxycycline (DOXY), which appears to successfully represses MMP2 and MMP9 activity after 72 hours treatment by zymography (**Figure S5E**). However, since doxycycline is a broad spectrum MMP inhibitor with potentially significant side effects, we also tested in our system a small molecule inhibitor, marimastat, which specifically targets the MMPs seen dysregulated in our model (including MMP2, MMP9, MMP14 and MMP7). Upon 4 days treatment with 8µM doxycycline (DOXY) or 1uM marimastat (MAR), disease BMEC stained for occludin and claudin-5 show a significant reduction of discontinuous and frayed junction compared to control (DMSO) (**Figure 5A,B).** Similar effects were seen in iECs treated with doxycycline or Marimastat (**Figure S5F,G**).

In addition, treatment with doxycycline or marimastat appeared to increase total occludin and claudin-5 protein levels by western blotting (**Figure 5C,D).** Remarkably, both doxycycline or marimastat treatment benefited on BMEC barrier properties as evidenced by significantly increasing TEER values (**Figure 5E**) and reducing the NaFl permeability percentage (**Figure 5F).**

We also looked at the effect of inhibiting MMPs by doxycycline and marimastat treatments on collagen IV deposition in *COL4A1/A2* hiPSC-derived MC and we found that collagen IV fluorescence levels detected by immunostaining in the *COL4A1/A2* decellularized ECM increased upon treatments compared to controls (**Figure 5G,H**). Doxycycline and marimastat treated disease MC cells also show a significant decreased migration rate at 24 hours (**Figure 5I,J)**, and lower apoptotic levels (**Figure 5K,L)** comparable to controls

(**Figure 1G).** These data establish a role for ECM remodelling due to MMPs caused by *COL4A1/A2* mutations and provide *in vitro* evidence that modulating specific MMPs may represent a therapeutic target for SVD.

Discussion

There is a critical need to develop new relevant models relevant to human SVD to provide mechanistic insights as well as a foundation to test potential treatments for this debilitating disorder. To address this, we characterised a novel *in vitro* model of human SVD produced by differentiating iPSC generated from patients with a *COL4A1* or a *COL4A2* SVD related mutation into MC.

We used *COL4A1/A2* patient derived hiPSC-MC in a co-culture system with brain microvascular endothelial-like cells to mimic the changes seen in patients' small vessels and to investigate underlying pathological mechanisms. Firstly, we observed increased expression of smooth muscle cells markers, such as *CNN1* and *ACTA2*, in *COL4A1/A2* MC at late stage of differentiation, which may suggest hypermuscularization as previously shown in a Col4a1 mouse model (Ratelade et al., 2020). Disease mural cells also showed an ECM defect including lower levels of extracellular collagen IV in agreement with previous findings from patient cells, indicating that SNPs in the triple helix-forming domain are likely to affect the protein conformation, which in turn may destabilize collagen IV deposition in the ECM (Jeanne et al., 2015; Murray et al., 2014). We also determined phenotypic changes in disease mural cells, including increased migration and apoptotic rates which parallel previous studies using primary patient fibroblasts (Murray et al., 2014). A loss of mural cells has been reported before and could be caused by several mechanisms, including ECM remodelling and endoplasmic reticulum stress (Ratelade et al., 2018, 2020).

Given the key strategic location of the ECM at the interface between blood and brain, a central aim of the study was to determine where COL4 disease influences barrier related properties. Interestingly, *COL4A1/A2* patient-derived MC exerted a detrimental effect on the endothelial barrier functions by a paracrine effect -evidenced by our transwell setup and with MC conditioned media treatment.

In this study, for the first time, we provided insight into the transcriptional features of *COL4A1/A2* patient-derived MC. Strikingly 15% of changes affected ECM proteins, including MMPs. Collagen IV is a substrate for the proteolytic activity of the gelatinases MMP2 and MMP9 and the matrilysin, MMP7. Increased MMP2 and MMP9 expression has been associated with breakdown of collagen type IV in both human and animal models (Roach et al., 2002; Rosell et al., 2008), as well as with degradation and cellular rearrangement of the endothelial tight junctions (Bauer et al., 2010; Liu et al., 2012; Yang et al., 2007). Recently, MMP7 has been found to correlate with BBB dysfunction following traumatic brain injury (Nichols et al., 2021). Moreover, MMPs are known to play a role in smooth muscle migratory behaviour and may facilitate MC migration in our *COL4A1/A2* model by promoting ECM proteins proteolysis (Underly et al., 2017). Interestingly, we observed a biphasic change for *MMP2* mRNA with expression levels increasing at later differentiation stage which corresponds with greater ECM deposition. This suggests that abnormal collagen IV deposition may contribute to higher MMPs activity which in turn could lead to increased cell death seen in our disease models.

These findings suggest MMPs could play a role in the ECM alterations in *COL4A1/A2* related SVD and could present a novel therapeutic opportunity. In support of this, targeting MMPs using the pan-MMP inhibitor, doxycycline, partially rescued the disease MC phenotypes, including promoting collagen IV extracellular levels, reducing migration and apoptotic levels, and improving BMEC/iECs tight junction abnormalities. In other studies, doxycycline was shown to reduced vascular remodelling and damage induced by cerebral

ischemia in a stroke animal model, the stroke-prone spontaneously hypertensive rats (Pires et al., 2011). However, doxycycline is a broad spectrum MMP inhibitor with potentially significant side effects. For this reason, we tested the small molecule inhibitor, marimastat, which specifically targets the MMPs seen dysregulated in our models. Marimastat was the first MMP inhibitor to be tested in clinical trials and now used for patients with different types of cancer (Thomas and Steward, 2005). Importantly, it was well tolerated by patients with short-term treatment.

Overall, major strengths of this work are 1) the generation of a new hiPSC-derived disease model for SVD, which replicates phenotypic changes observed in patients and *Col4a1* animal model, including ECM abnormalities; 2) this disease-relevant model can be used as new tool for the analysis of signalling pathways to identify therapeutic targets, such as specific MMP and 3) to screen and test for potential drugs against SVD.

Our work has limitations. First, the *COL4A2* hiPSC line was generated from the asymptomatic father of the patient. Previously, it has been shown that the father's fibroblasts lack some of the prosperities seen in the patients' ones. However, in our model, *COL4A2* phenotypic changes are comparable to the *COL4A1* line (symptomatic), and this may be due to the use of relevant cell types to investigate these changes. Secondly, generating representative brain endothelial cells that possess endothelial identity while replicating the BBB properties, including elevated TEER and small molecule low permeability, has been a challenge highlighted in recent hiPSC work (Lu et al., 2021). We initially used the Hollman *et al* protocol, which originates from the Lippman lab (Hollmann et al., 2017). These cells display high TEER, however, they do also express epithelial-related genes and lack angiogenic properties (Lu et al., 2021). In view of these limitations, we then successfully validated our results using a generic endothelial protocol (Orlova et al., 2014b), however this lacks barrier-like functions. Further research is required to improve the current protocols for generation of BMEC cells, based on the emerging understanding of the BBB from single-cells sequencing studies (Garcia et al., 2022).

In conclusion, our novel hiPSC-derived mural cells model of *COL4A1/A2* mutations, supports a key role of the ECM in SVD and suggests that targeting ECM-related proteins like MMPs may be a promising potential therapeutic option.

Experimental procedures

Resource availability

Corresponding author

Further information and requests for resources and reagents should be directed to and will be fulfilled by the corresponding author, Alessandra Granata (ag686@cam.ac.uk).

Materials availability

This study did not generate new unique reagents. Materials are listed in experimental procedures, supplemental information and can be requested from the corresponding author.

Data and code availability

The RNAseq data generated during this study has been deposited in the University of Cambridge repository (https://doi.org/10.17863/CAM.100127).

Experimental methods

HiPSC culture

All the hiPSC lines use for this study are listed in **Table S1.** Full culture condition and medium formulation can be found in the supplemental information.

HiPSC differentiation into mural cells

hiPSC were differentiated into mural cells of neural crest origin (NC) using a previously described protocol (Cheung et al., 2012; Serrano et al., 2019). Full culture condition and medium formulation can be found in the supplemental information.

HiPSC differentiation into BMEC and iECs

hiPSCs were differentiated to brain microvascular endothelial-like cells (BMEC) as previously described, with minor modifications (Hollmann et al., 2017). hiPSC-ECs (iECs) were differentiated using a previously reported protocol with minor modifications (Orlova et al., 2014b). Full culture condition and medium formulation can be found in the supplemental information.

Transwell co-culture

Either 12-well or 24-well Transwells® (Corning® 0.4 µm pore; Sigma Aldrich) were coated on the apical and basolateral side with collagen IV/fibronectin. hiPSC-mural cells were dissociated with TrypLE and seeded onto the plate bottom of the Transwell® coated with 0.1% Gelatin. After incubation for 1 hour, hiPSC-BMEC were dissociated and the seeded onto the apical side. The next day, Transwells® with BMEC with(out) mural cells were maintained without any further medium changes for up to 6 days before analyses.

Paracrine. MC were serum starved for 4 days. At day 5, the MC serum-starved conditioned media was added to BMEC seeded onto collagen IV/fibronectin coated 24-well Transwells® for TEER and NaFl analyses or 24-well plates for immunostaining assay. Initial TEER measurement was taken after 24h and afterwards on daily basis. For NaFl and immunostaining assays, BMEC were treated with condition media, refreshed every other day, for 6 days.

BMEC functional assays

TEER. Transendothelial Electrical Resistance (TEER) measurements were taken every 24 hours, from day 1 to day 6 of subculture of BMEC onto Transwells® using an EVOM2 Voltohmmeter/STX2 electrodes (World Precision Instruments). The STX2 electrode was positioned within the well and the resistance (Ω) was recorded three times to calculate the mean resistance. All values are given as $\Omega x cm^2$ after subtracting the resistance of an empty coated Transwell® well maintained in the same culture media (blank) and multiplying by the surface area ($0.33cm^2$) as described previously (Lee et al., 2018). TEER was expressed as peak value.

NaFl. At 2 days post-subculture of BMEC onto 24 well Transwells®, spent media was removed from the upper chamber of the Transwell® and replaced with 600µl of Sodium Fluorescein (NaFl, Sigma-Aldrich 1mg/ml) diluted 1:100 in endothelial serum-free media with B27. Samples of 100µl were taken from the basolateral side every two hours for eight hours. Raw fluorescence was measured with a TECAN Infinite M200 Pro plate reader (excitation wavelength of 460nm and emission 515nm; gain of 50, 25 flashes; z-position of 20000). Quantification was represented as percentage of total fluorescence relative to empty coated Transwell® well (blank) as previously (Lee et al., 2018).

Doxycycline and Marimastat treatments

hiPSC-derived mural cells were treated with doxycycline (10uM; Sigma) or marimastat (provided by AstraZeneca; 1uM in DMSO) in DMEM+10% FBS for 4 days, with media change every other day, and then harvested for analyses. BMEC/iECs were treated with 8uM of doxycycline or marimastat (1uM) in EC medium, with media change every other day, and collected at 24h and 72h for zymography and at day 6 for immunostaining and western blotting analysis. TEER measurements were taken every 24 hours from day 1 to day 6 of subculture of BMEC onto Transwells in media supplemented with doxycycline or

marimastat. NaF permeability assay was performed after 6 days of doxycycline or marimastat treatment.

RNA sequencing

Samples preparation. Three sets (biological replicates) of hiPSC-derived mural cells grown in DMEM+10%serum for 1 weeks were harvested. Total RNA was isolated from cells using RNeasy Mini Kit (QIAGEN). Upon ribosomal RNA depletion, libraries were prepared using a NEBNext RNA library Prep kit (Illumina). The samples were run on an Novaseq6000 S4 lane and150 bp paired-end reads were generated.

Data analysis. The resulting base call files were converted to fastq files using the bcl2fastq program. Alignment in STAR (2.7.10a) using a modified version of the ENCODE-DCC RNAseq pipeline annotated using GENCODE v39 (hg38) was performed (Dobin et al., 2013). Gene-level RNA expression quantification was performed with RSEM (Li and Dewey, 2011).

Differential expression analyses were carried out using DESeq2 in R v4.0.4 (Love et al., 2014). We specified a false discovery rate of 5% and applied a Bayesian shrinkage estimator to effect sizes using approximation of the posterior for individual coefficients. Results were visualised using the EnhancedVolcano package.

Enrichment of gene-sets of interest was calculated using logistic regression. We used data from human samples to categorise genes associated with the ECM (Pokhilko et al., 2021) and matrix metalloproteinases (**Table S5**). Pathways enrichment analysis was performed using the Reactome (**Table S6**) (Wu and Haw, 2017). We chose a 5% FDR to indicate statistical significance.

Statistical analysis.

Data, expressed as means ± SD, were analyzed statistically using SPSS 22.0 software. Unpaired Student's t test for two-group comparisons or one-way ANOVA followed by LSD multiple comparisons was performed using GraphPad Prism 9.00 (GraphPad Software Inc.) to analyze the significant difference, which was indicated as ns (not significant) P>0.05; * P<0.05; **P<0.01; ***P<0.001; ****P<0.0001. The "n," noted in the figure legends, represents the replicated number of biological experiments. All data are representative of at least three independent experiments.

Acknowledgments

We thank the NIHR Cambridge BRC Cell Phenotyping Hub and the Flow cytometry core facilities at the Cambridge Institute for Medical Research (CIMR). We thank Dr David Smith, Principal scientist at AstraZeneca R&D, for providing the small molecule, marimastat, through the Open Innovation platform. We also thank Professor L. Vallier and the hiPSC core facility for generating the *COL4A1* hiPSC line.

The present work was supported by a Stroke Association priority programme award in Advancing Care and Treatment of Vascular Dementia (grant reference 16VAD_04) in partnership with the British Heart Foundation and Alzheimer's Society to KH and SA/TVA/AG/HM/SS/TW. AG is supported by the MRF mid-career fellowship (RG RG98759). This research was funded by the British Heart Foundation via the Cambridge British Heart Foundation Centre of Research Excellence (RE/18/1/34212) and a British Heart Foundation programme grant (RG/F/22/110052). Infrastructural support was provided by the Cambridge University Hospitals NIHR Biomedical Research Centre (BRC-1215-20014). HSM is supported by a NIHR Senior Investigator Award. The views expressed are those of the authors and not necessarily those of the NIHR or the Department of Health and Social Care.

Author contributions

AG contribute to the conception, design and interpretation of the hiPSC model data and to the drafting of the article. MA and MGT equally contributed to the acquisition and analysis of the data. SB undertook the transcriptomic data analysis. KP helped with hiPSC differentiation and establishing the co-culture and paracrine model. TVA and LKF undertook the mouse aorta dissection and analysis, KH and TVA provided critical reading of the manuscript. CV and MA are the clinicians for the patient with the *COL4A2* mutation. HSM is the clinician for the patient with *COL4A1* mutation, contributed to the revision of the article and the supervision of all studies. All authors contributed to the article and approved the submitted version.

Declaration of interests

None

References

van Agtmael, T., Schlötzer-Schrehardt, U., McKie, L., Brownstein, D.G., Lee, A.W., Cross, S.H., Sado, Y., Mullins, J.J., Pöschl, E., and Jackson, I.J. (2005). Dominant mutations of Col4a1 result in basement membrane defects which lead to anterior segment dysgenesis and glomerulopathy. Hum Mol Genet *14*, 3161–3168.

Bauer, A.T., Bürgers, H.F., Rabie, T., and Marti, H.H. (2010). Matrix metalloproteinase-9 mediates hypoxia-induced vascular leakage in the brain via tight junction rearrangement. J Cereb Blood Flow Metab *30*, 837. h

Candelario-Jalil, E., Thompson, J., Taheri, S., Grossetete, M., Adair, J.C., Edmonds, E., Prestopnik, J., Wills, J., and Rosenberg, G.A. (2011). Matrix metalloproteinases are associated with increased blood-brain barrier opening in vascular cognitive impairment. Stroke *42*, 1345–1350.

Cheung, C., Bernardo, A.S., Trotter, M.W.B., Pedersen, R.A., and Sinha, S. (2012). Generation of human vascular smooth muscle subtypes provides insight into embryological origin-dependent disease susceptibility. Nat Biotechnol *30*, 165–173.

Chung, J., Consortium, I.S.G., Marini, S., Consortium, I.S.G., Pera, J., Consortium, I.S.G., Norrving, B., Consortium, I.S.G., Jimenez-Conde, J., Consortium, I.S.G., et al. (2019). Genome-wide association study of cerebral small vessel disease reveals established and novel loci. Brain *142*, 3176–3189.

Chung, J., Marini, S., Pera, J., Norrving, B., Jimenez-Conde, J., Roquer, J., Fernandez-Cadenas, I., Tirschwell, D.L., Selim, M., Brown, D.L., et al. Genome-wide association study of cerebral small vessel disease reveals established and novel loci on behalf of the International Stroke Genetics Consortium. https://doi.org/10.1093/brain/awz233.

Clark, A.W., Krekoski, C.A., Bou, S.S., Chapman, K.R., and Edwards, D.R. (1997). Increased gelatinase A (MMP-2) and gelatinase B (MMP-9) activities in human brain after focal ischemia. Neurosci Lett *238*, 53–56

Dobin, A., Davis, C.A., Schlesinger, F., Drenkow, J., Zaleski, C., Jha, S., Batut, P., Chaisson, M., and Gingeras, T.R. (2013). STAR: ultrafast universal RNA-seq aligner. Bioinformatics *29*, 15–21.

Garcia, F.J., Sun, N., Lee, H., Godlewski, B., Mathys, H., Galani, K., Zhou, B., Jiang, X., Ng, A.P., Mantero, J., et al. (2022). Single-cell dissection of the human brain vasculature. Nature 2022 603:7903 *603*, 893–899.

Gorelick, P.B., Scuteri, A., Black, S.E., Decarli, C., Greenberg, S.M., Iadecola, C., Launer, L.J., Laurent, S., Lopez, O.L., Nyenhuis, D., et al. (2011). Vascular contributions to cognitive impairment and dementia: a statement for healthcare professionals from the american heart association/american stroke association. Stroke *42*, 2672–2713.

Gould, D.B., Phalan, F.C., Breedveld, G.J., van Mil, S.E., Smith, R.S., Schimenti, J.C., Aguglia, U., van der Knaap, M.S., Heutink, P., and John, S.W.M. (2005). Mutations in Col4a1 cause perinatal cerebral hemorrhage and porencephaly. Science *308*, 1167–1171.

Hollmann, E.K., Bailey, A.K., Potharazu, A. v, Neely, M.D., Bowman, A.B., and Lippmann, E.S. (2017). Accelerated differentiation of human induced pluripotent stem cells to blood-brain barrier endothelial cells. Fluids Barriers CNS *14*, 9.
Hussain, B., Fang, C., and Chang, J. (2021). Blood-Brain Barrier Breakdown: An Emerging Biomarker of Cognitive Impairment in Normal Aging and Dementia. Front Neurosci *15*.
Jeanne, M., Labelle-Dumais, C., Jorgensen, J., Kauffman, W.B., Mancini, G.M., Favor, J., Valant, V., Greenberg, S.M., Rosand, J., and Gould, D.B. (2012). COL4A2 mutations impair COL4A1 and COL4A2 secretion and cause hemorrhagic stroke. Am J Hum Genet *90*, 91–101.
Jeanne, M., Jorgensen, J., and Gould, D.B. (2015). Molecular and Genetic Analyses of Collagen Type IV Mutant Mouse Models of Spontaneous Intracerebral Hemorrhage Identify Mechanisms for Stroke Prevention. Circulation *131*, 1555–1565.
Jones, F.E., Bailey, M.A., Murray, L.S., Lu, Y., McNeilly, S., SchloÌtzer-Schrehardt, U., Lennon, R., Sado, Y., Brownstein, D.G., Mullins, J.J., et al. (2016). ER stress and basement membrane defects combine to cause glomerular and tubular renal disease resulting from Col4a1 mutations in mice. DMM Disease Models and Mechanisms *9*, 165–176.
Jones, F.E., Murray, L.S., McNeilly, S., Dean, A., Aman, A., Lu, Y., Nikolova, N., Malomgré, R., Horsburgh, K., Holmes, W.M., et al. (2019). 4-Sodium phenyl butyric acid has both efficacy and counter-indicative effects in the treatment of Col4a1 disease. Hum Mol Genet *28*, 628.
Joutel, A., and Faraci, F.M. (2014). Cerebral small vessel disease: insights and opportunities from mouse models of collagen IV-related small vessel disease and cerebral autosomal dominant arteriopathy with subcortical infarcts and leukoencephalopathy. Stroke *45*, 1215–1221.
Joutel, A., Haddad, I., Ratelade, J., and Nelson, M.T. (2016). Perturbations of the cerebrovascular matrisome: A convergent mechanism in small vessel disease of the brain? Journal of Cerebral Blood Flow & Metabolism *36*, 143–157.
Kuuluvainen, L., Mönkäre, S., Kokkonen, H., Zhao, F., Verkkoniemi-Ahola, A., Schleutker, J., Hakonen, A.H., Hartikainen, P., Pöyhönen, M., and Myllykangas, L. (2021). COL4A1 and COL4A2 Duplication Causes Cerebral Small Vessel Disease with Recurrent Early Onset Ischemic Strokes. Stroke E624–E625.
Lam, B.Y., Cai, Y., Akinyemi, R., Biessels, G.J., Brink, H. van den, Chen, C.L., Cheung, C.W., Chow, K.N., Chung, H.K., Duering, M., et al. (2022). The global burden of cerebral small vessel disease in low- and middle-income countries: A systematic review and meta-analysis. Int J Stroke 174749302211370.
Lee, C.A.A., Seo, H.S., Armien, A.G., Bates, F.S., Tolar, J., and Azarin, S.M. (2018). Modeling and rescue of defective blood-brain barrier function of induced brain microvascular endothelial cells from childhood cerebral adrenoleukodystrophy patients. Fluids Barriers CNS *15*.
Li, B., and Dewey, C.N. (2011). RSEM: Accurate transcript quantification from RNA-Seq data with or without a reference genome. BMC Bioinformatics *12*, 1–16.
Liu, J., Jin, X., Liu, K.J., and Liu, W. (2012). Matrix metalloproteinase-2-mediated occludin degradation and caveolin-1-mediated claudin-5 redistribution contribute to blood-brain barrier damage in early ischemic stroke stage. J Neurosci *32*, 3044–3057.
Love, M.I., Huber, W., and Anders, S. (2014). Moderated estimation of fold change and dispersion for RNA-seq data with DESeq2. Genome Biol *15*, 1–21.
Lu, T.M., Houghton, S., Magdeldin, T., Barcia Durán, J.G., Minotti, A.P., Snead, A., Sproul, A., Nguyen, D.H.T., Xiang, J., Fine, H.A., et al. (2021). Pluripotent stem cell-derived epithelium misidentified as brain microvascular endothelium requires ETS factors to acquire vascular fate. Proc Natl Acad Sci U S A *118*, e2016950118.

Malik, R., Chauhan, G., Traylor, M., Sargurupremraj, M., Okada, Y., Mishra, A., Rutten-Jacobs, L., Giese, A.-K., van der Laan, S.W., Gretarsdottir, S., et al. (2018). Multiancestry genome-wide association study of 520,000 subjects identifies 32 loci associated with stroke and stroke subtypes. Nat Genet 1.
Mancuso, M., Arnold, M., Bersano, A., Burlina, A., Chabriat, H., Debette, S., Enzinger, C., Federico, A., Filla, A., Finsterer, J., et al. (2020). Monogenic cerebral small-vessel diseases: diagnosis and therapy. Consensus recommendations of the European Academy of Neurology. Eur J Neurol *27*, 909–927.
Murray, L.S., Lu, Y., Taggart, A., Van Regemorter, N., Vilain, C., Abramowicz, M., Kadler, K.E., and Van Agtmael, T. (2014). Chemical chaperone treatment reduces intracellular accumulation of mutant collagen IV and ameliorates the cellular phenotype of a COL4A2 mutation that causes haemorrhagic stroke. Hum Mol Genet *23*, 283–292.
Nichols, P., Urriola, J., Miller, S., Bjorkman, T., Mahady, K., Vegh, V., Nasrallah, F., and Winter, C. (2021). Blood-brain barrier dysfunction significantly correlates with serum matrix metalloproteinase-7 (MMP-7) following traumatic brain injury.
Nitta, T., Hata, M., Gotoh, S., Seo, Y., Sasaki, H., Hashimoto, N., Furuse, M., and Tsukita, S. (2003). Size-selective loosening of the blood-brain barrier in claudin-5-deficient mice. J Cell Biol *161*, 653–660.
Orlova, V. v., Drabsch, Y., Freund, C., Petrus-Reurer, S., van den Hil, F.E., Muenthaisong, S., ten Dijke, P., and Mummery, C.L. (2014a). Functionality of endothelial cells and pericytes from human pluripotent stem cells demonstrated in cultured vascular plexus and zebrafish xenografts. Arterioscler Thromb Vasc Biol *34*, 177–186.
Orlova, V. v., van den Hil, F.E., Petrus-Reurer, S., Drabsch, Y., ten Dijke, P., and Mummery, C.L. (2014b). Generation, expansion and functional analysis of endothelial cells and pericytes derived from human pluripotent stem cells. Nat Protoc *9*, 1514–1531.
Pan, R., Yu, K., Weatherwax, T., Zheng, H., Liu, W., and Liu, K.J. (2017). Blood Occludin Level as a Potential Biomarker for Early Blood Brain Barrier Damage Following Ischemic Stroke. Sci Rep *7*.
Persyn, E., Hanscombe, K.B., Howson, J.M.M., Lewis, C.M., Traylor, M., and Markus, H.S. (2020). Genome-wide association study of MRI markers of cerebral small vessel disease in 42,310 participants. Nature Communications 2020 11:1 *11*, 1–12.
Pires, P.W., Rogers, C.T., Mcclain, J.L., Garver, H.S., Fink, G.D., and Dorrance, A.M. (2011). Doxycycline, a matrix metalloprotease inhibitor, reduces vascular remodeling and damage after cerebral ischemia in stroke-prone spontaneously hypertensive rats. Am J Physiol Heart Circ Physiol *301*, 87–97.
Pokhilko, A., Brezzo, G., Handunnetthi, L., Heilig, R., Lennon, R., Smith, C., Allan, S.M., Granata, A., Sinha, S., Wang, T., et al. (2021). Global proteomic analysis of extracellular matrix in mouse and human brain highlights relevance to cerebrovascular disease. J Cereb Blood Flow Metab *41*, 2423–2438.
Rannikmäe, K., Davies, G., Thomson, P.A., Bevan, S., Devan, W.J., Falcone, G.J., Traylor, M., Anderson, C.D., Battey, T.W.K., Radmanesh, F., et al. (2015). Common variation in COL4A1/COL4A2 is associated with sporadic cerebral small vessel disease. Neurology *84*, 918–926.
Ratelade, J., Mezouar, N., Domenga-Denier, V., Rochey, A., Plaisier, E., and Joutel, A. (2018). Severity of arterial defects in the retina correlates with the burden of intracerebral haemorrhage in COL4A1-related stroke. J Pathol *244*, 408–420.
Ratelade, J., Klug, N.R., Lombardi, D., Angelim, M.K.S.C., Dabertrand, F., Dabertrand, F., Domenga-Denier, V., Salman, R.A.S., Smith, C., Gerbeau, J.F., et al. (2020). Reducing Hypermuscularization of the Transitional Segment between Arterioles and Capillaries Protects against Spontaneous Intracerebral Hemorrhage. Circulation 2078–2094.
Roach, D.M., Fitridge, R.A., Laws, P.E., Millard, S.H., Varelias, A., and Cowled, P.A. (2002). Up-regulation of MMP-2 and MMP-9 Leads to Degradation of Type IV Collagen

During Skeletal Muscle Reperfusion Injury; Protection by the MMP Inhibitor, Doxycycline. European Journal of Vascular and Endovascular Surgery *23*, 260–269.
Rosell, A., Cuadrado, E., Ortega-Aznar, A., Hernández-Guillamon, M., Lo, E.H., and Montaner, J. (2008). MMP-9-positive neutrophil infiltration is associated to blood-brain barrier breakdown and basal lamina type IV collagen degradation during hemorrhagic transformation after human ischemic stroke. Stroke *39*, 1121–1126.
Serrano, F., Bernard, W.G., Granata, A., Iyer, D., Steventon, B., Kim, M., Vallier, L., Gambardella, L., and Sinha, S. (2019). A Novel Human Pluripotent Stem Cell-Derived Neural Crest Model of Treacher Collins Syndrome Shows Defects in Cell Death and Migration. Stem Cells Dev *28*.
Shah, S., Kumar, Y., McLean, B., Churchill, A., Stoodley, N., Rankin, J., Rizzu, P., van der Knaap, M., and Jardine, P. (2010). A dominantly inherited mutation in collagen IV A1 (COL4A1) causing childhood onset stroke without porencephaly. Eur J Paediatr Neurol *14*, 182–187. https://doi.org/10.1016/J.EJPN.2009.04.010.
Siitonen, M., Börjesson-Hanson, A., Pöyhönen, M., Ora, A., Pasanen, P., Bras, J., Kern, S., Kern, J., Andersen, O., Stanescu, H., et al. (2017). Multi-infarct dementia of Swedish type is caused by a 3'UTR mutation of COL4A1. Brain *140*, e29.
Smith, E.E., and Markus, H.S. (2020). New Treatment Approaches to Modify the Course of Cerebral Small Vessel Diseases. Stroke *51*, 38–46.
Thomas, A.L., and Steward, W.P. (2005). Marimastat: the clinical development of a matrix metalloproteinase inhibitor. Http://Dx.Doi.Org/10.1517/13543784.9.12.2913 *9*, 2913–2922.
Traylor, M., Persyn, E., Tomppo, L., Klasson, S., Abedi, V., Bakker, M.K., Torres, N., Li, L., Bell, S., Rutten-Jacobs, L., et al. (2021). Genetic basis of lacunar stroke: a pooled analysis of individual patient data and genome-wide association studies. Lancet Neurol *20*, 351–361..
Underly, R.G., Levy, M., Hartmann, D.A., Grant, R.I., Watson, A.N., and Shih, A.Y. (2017). Pericytes as Inducers of Rapid, Matrix Metalloproteinase-9-Dependent Capillary Damage during Ischemia. J Neurosci *37*, 129–140.
Verdura, E., Hervé, D., Bergametti, F., Jacquet, C., Morvan, T., Prieto-Morin, C., Mackowiak, A., Manchon, E., Hosseini, H., Cordonnier, C., et al. (2016). Disruption of a miR-29 binding site leading to COL4A1 upregulation causes pontine autosomal dominant microangiopathy with leukoencephalopathy. Ann Neurol *80*, 741–753.
Wallin, A., Kapaki, E., Boban, M., Engelborghs, S., Hermann, D.M., Huisa, B., Jonsson, M., Kramberger, M.G., Lossi, L., Malojcic, B., et al. (2017). Biochemical markers in vascular cognitive impairment associated with subcortical small vessel disease - A consensus report. BMC Neurology 2017 17:1 *17*, 1–12.
Wardlaw, J.M., Allerhand, M., Doubal, F.N., Hernandez, M.V., Morris, Z., Gow, A.J., Bastin, M., Starr, J.M., Dennis, M.S., and Deary, I.J. (2014). Vascular risk factors, large-artery atheroma, and brain white matter hyperintensities. Neurology *82*, 1331–1338.
Wardlaw, J.M., Smith, C., and Dichgans, M. (2019). Small vessel disease: mechanisms and clinical implications. Lancet Neurol *18*, 684–696.
Wu, G., and Haw, R. (2017). Functional interaction network construction and analysis for disease discovery. Methods in Molecular Biology *1558*, 235–253.
Yang, Y., Estrada, E.Y., Thompson, J.F., Liu, W., and Rosenberg, G.A. (2007). Matrix metalloproteinase-mediated disruption of tight junction proteins in cerebral vessels is reversed by synthetic matrix metalloproteinase inhibitor in focal ischemia in rat. Journal of Cerebral Blood Flow and Metabolism *27*, 697–709.

Figure Titles and Legends

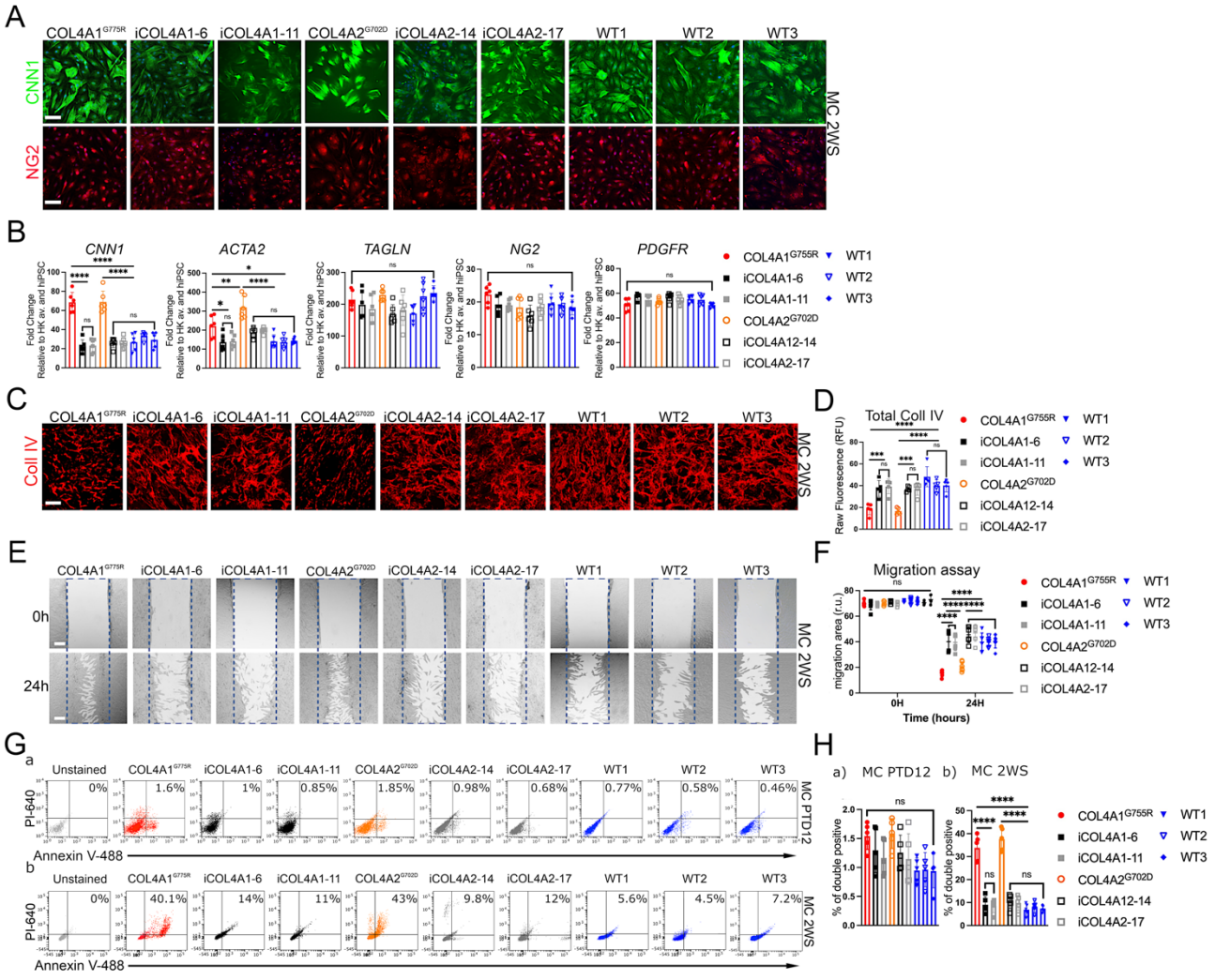

Figure 1. COL4A1^{G755R}, COL4A2^{G702D} hiPSC-derived mural cells show abnormal collagen IV and phenotypic changes.

A) Immunostaining for Calponin (CNN1) and Nerve/glial antigen 2 (NG2) in hiPSC-derived mural cells (MC) cultured for 2 weeks in serum containing media (2WS) for COL4A1^{G755R}, COL4A2^{G702D}, 2 isogenic sub-clones for A1 (iCOL4A1-6 and iCOL4A1-11) and A2 (iCOL4A2-14 and iCOL4A2-17) and three healthy controls (WT1, WT2, WT3; **Table S1**). **B)** RT-qPCR analysis for MC markers, including *CNN1, ACTA2, TAGLN, NG2 and PDGFR* (n=6). **C)** Immunostaining for collagen IV in the ECM of mural cells show significant decreased levels in COL4A1^{G755R} and COL4A2^{G702D} when quantified as total fluorescence **(D)** compared to isogenic and WT controls (n=6). **E)** Representative images of scratch assays for hiPSC-MC and **(F)** quantification of the areas showing increased migration rate for COL4A1/A2 mutant MC compared to controls (n=6). **G)** Flow cytometric analysis of Annexin V-488 and propidium iodide (PI-640) in hiPSC-MC after 12 days of differentiation in PDGFBB+TGF-β1 (PTD12, early stage; **a**) and at late stage (2WS; **b**) show higher apoptotic rate in COL4A1/A2 mutant compared to control MC lines at 2WS (n=5) (**H**). Nuclei were stained with DAPI; scale bar=100µm. MC=neural crest-derived mural cells. The results are presented as means ± SD of n independent experiments *P<0.05; **P<0.01; ***P<0.001; ****P<0.0001; ns (not significant). Statistical analysis was performed by 2-way ANOVA with Tukey's multiple comparison test.

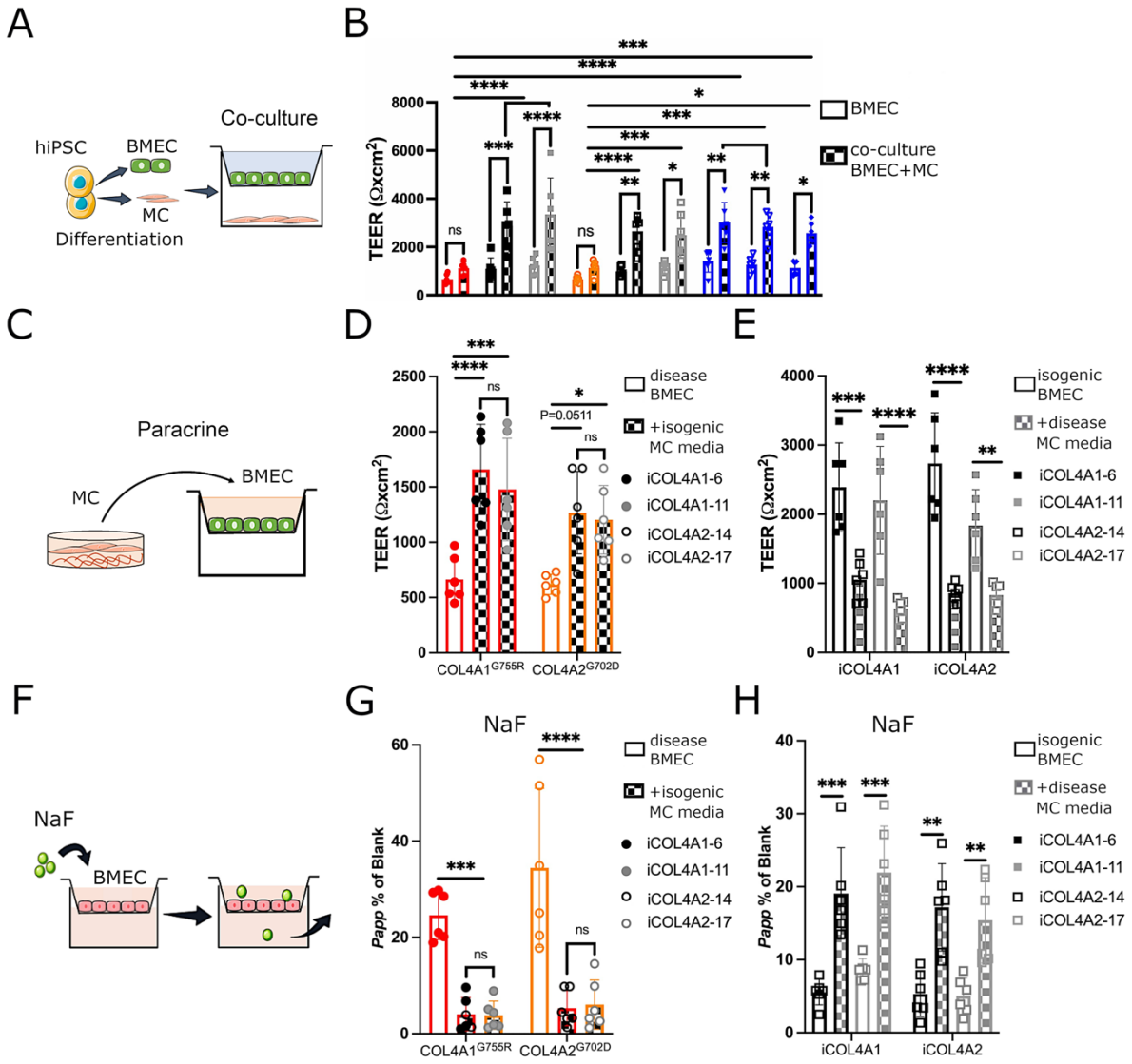

669
670
671 **Figure 2. hiPSC-derived mural cells contribute to barrier function in a Transwell co-**
672 **culture system and COL4A1/A2 lines exert a detrimental effect.**
673 **A)** Schematic of co-culture with hiPSC-derived mural cells (MC) and brain microvascular
674 endothelial-like cells (BMEC) in a Transwell device. **B)** Transendothelial electrical
675 resistance (TEER) peak values expressed as resistance (Ω) x cm^2 for hiPSC-derived
676 BMEC in co-culture with MC increases compared to BMEC alone for isogenic iCOL4A1/A2
677 and WTs (n=6). **C)** Schematic of the MC paracrine experiment with $COL4A1^{G755R}$ and
678 $COL4A2^{G702D}$ BMEC TEER values benefiting from treatment with isogenic MC conditioned
679 media **(D)** (n=6); while isogenic BMEC show decreased TEER values upon treatment with
680 disease COL4A1/A2 MC conditioned media (n=6) **(E). F)** Schematic of the sodium
681 fluorescein (NaF) permeability assay in transwell setting. Isogenic MC paracrine effect
682 positively reduce BMEC permeability in $COL4A1^{G755R}$ and $COL4A2^{G702D}$ lines after 6 days
683 treatment (n=6) **(G)**; while disease MC conditioned media treated isogenic BMEC show
684 increased permeability to NaF compared to untreated BMEC (n=6) **(H)**. TEER=
685 transendothelial electrical resistance; NaF= sodium fluorescein; *Papp*=apparent
686 permeability. The results are presented as means ± SD of n independent experiments
687 *P<0.05; **P<0.01; ***P<0.001; ****P<0.0001; ns (not significant). Statistical analysis was
688 performed by 2-way ANOVA with Tukey's multiple comparison test.
689

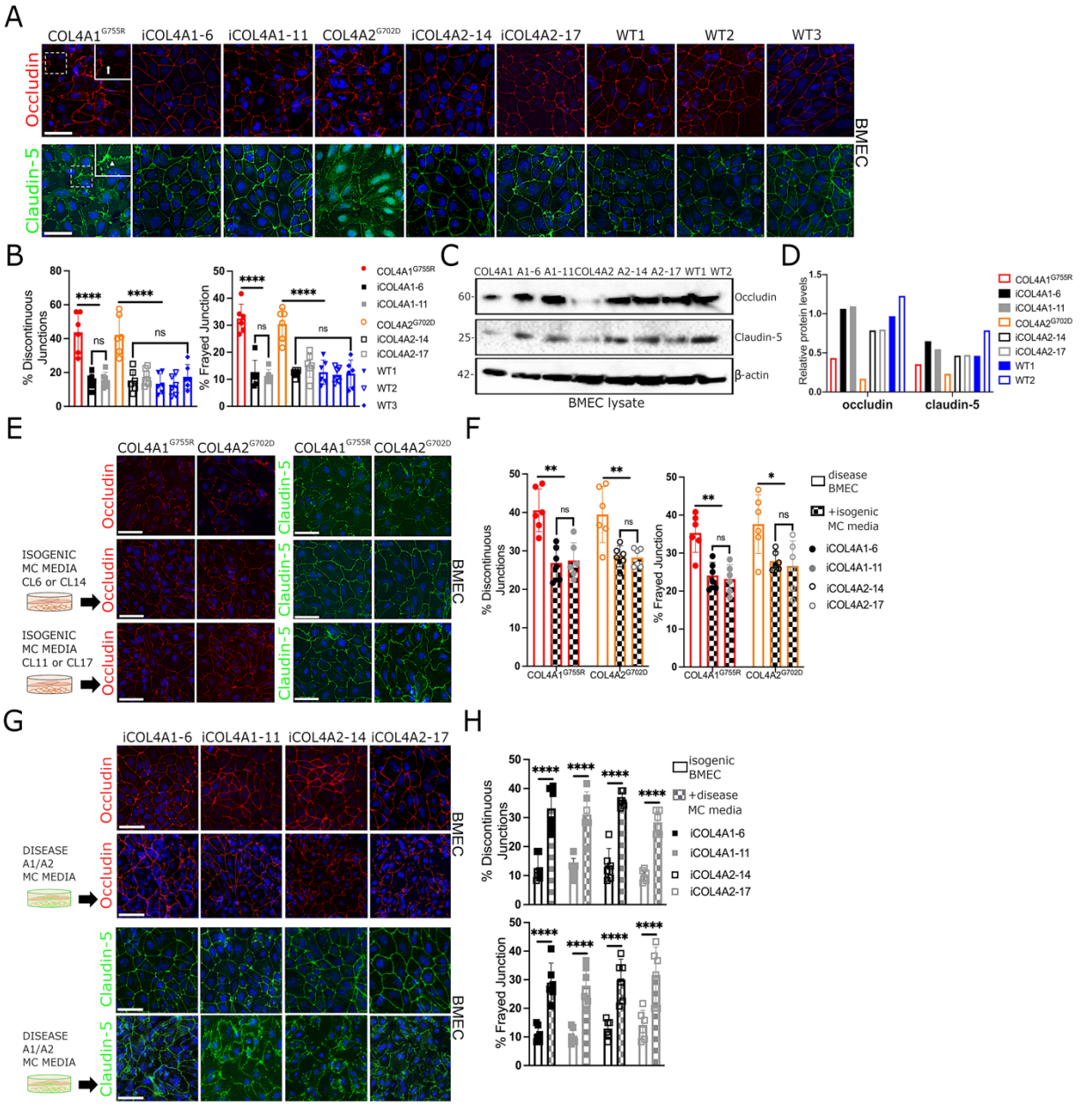

690
691
692 **Figure 3. COL4A1/A2 mural cells contribute to endothelial tight junction**
693 **abnormalities by paracrine effect.**
694 **A)** Junctional staining for occludin and claudin-5 in hiPSC-derived BMEC lines cultured
695 alone showing discontinuous junction (white arrow) and frayed junction (white arrowed) in
696 zoom-in insert. **B)** Quantification of discontinuous and frayed junctions show higher
697 percent in COL4A1^{G755R} and COL4A2^{G702D} lines compared to controls (n=6). **C-D**) Western
698 blotting analysis and bands quantification show decreased total protein levels for occludin
699 and claudin-5 in COL4A1^{G755R} and COL4A2^{G702D} derived BMEC compared to controls (A1
700 and A2 ISO) and WT1 and WT2. β-actin was used as loading controls (representative blot
701 of n=3). **E-F)** Immunostaining analysis of COL4A1^{G755R} and COL4A2^{G702D} BMEC tight
702 junctions (occludin and claudin-5) upon 4 days treatment with isogenic MC conditioned
703 media show less discontinuous and frayed junctions (n=6). **G-H)** Isogenic BMEC show
704 increased percent of junctions abnormalities upon treatment with disease MC conditioned
705 media (n=6). Nuclei were stained with DAPI; scale bar=100μm. The results are presented
706 as means ± SD of n independent experiments *P<0.05; **P<0.01; ***P<0.001;
707 ****P<0.0001; ns (not significant). Statistical analysis was performed by 2-way ANOVA
708 with Tukey's multiple comparison test.

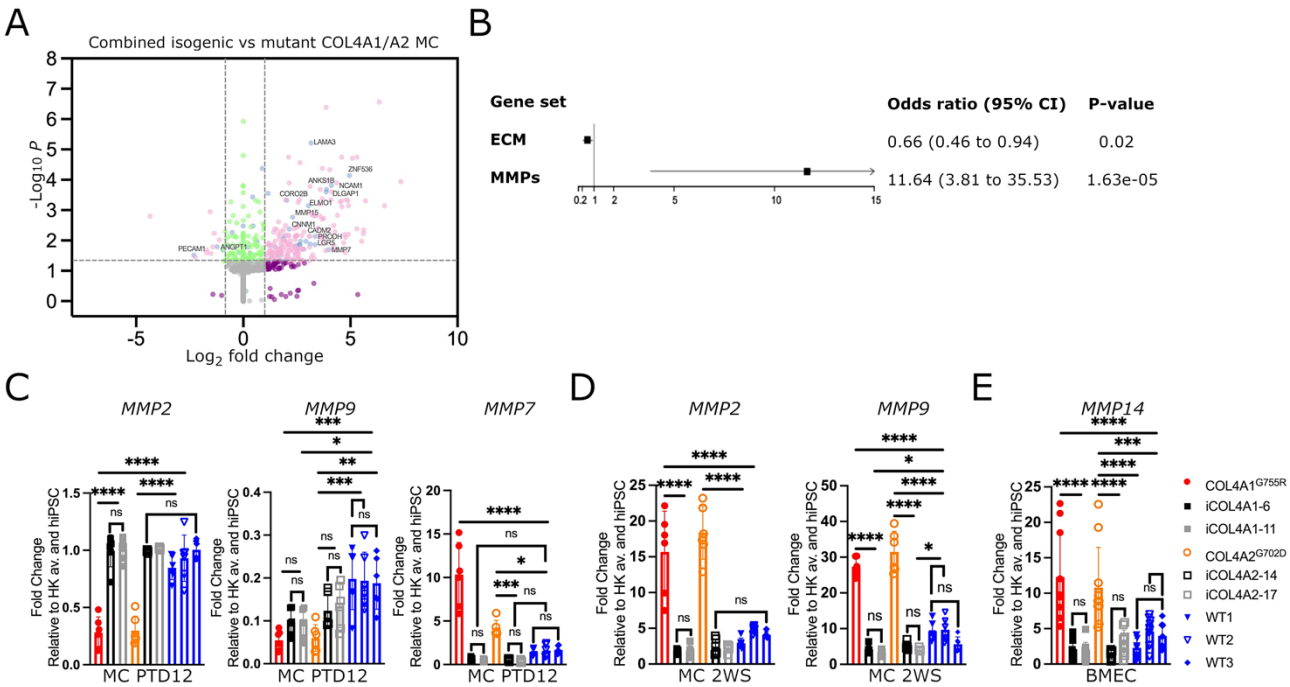

Figure 4. Transcriptomic analysis shows ECM abnormalities in COL4A1/A2 MC lines and MMPs upregulation.

A) Volcano plot depicting differentially expressed genes in combined COL4A1^{G755R} and COL4A2^{G702D} compared to isogenic MC; matrisome proteins with larger fold changes are labelled and **B)** forest plot shows significant enrichment for ECM and MMPs in diseased MC**. C-D)** RT-qPCR analysis performed at PTD12 and 2WS shows biphasic expression for *MMP2* at mRNA levels in COL4A1^{G755R} and COL4A2^{G702D} MC and higher levels for MMP7 and MMP9 at PTD12 and 2WS respectively in COL4A1^{G755R} and COL4A2^{G702D} MC compared to the isogenic and WT controls (n=6). **E)** *MMP14* mRNA was found higher in COL4A1/A2 compared to isogenic hiPSC-BMEC lines (n=10). The results are presented as means ± SD of n independent experiments *P<0.05; **P<0.01; ***P<0.001; ****P<0.0001; ns (not significant). Statistical analysis was performed by 2-way ANOVA with Tukey's multiple comparison test.

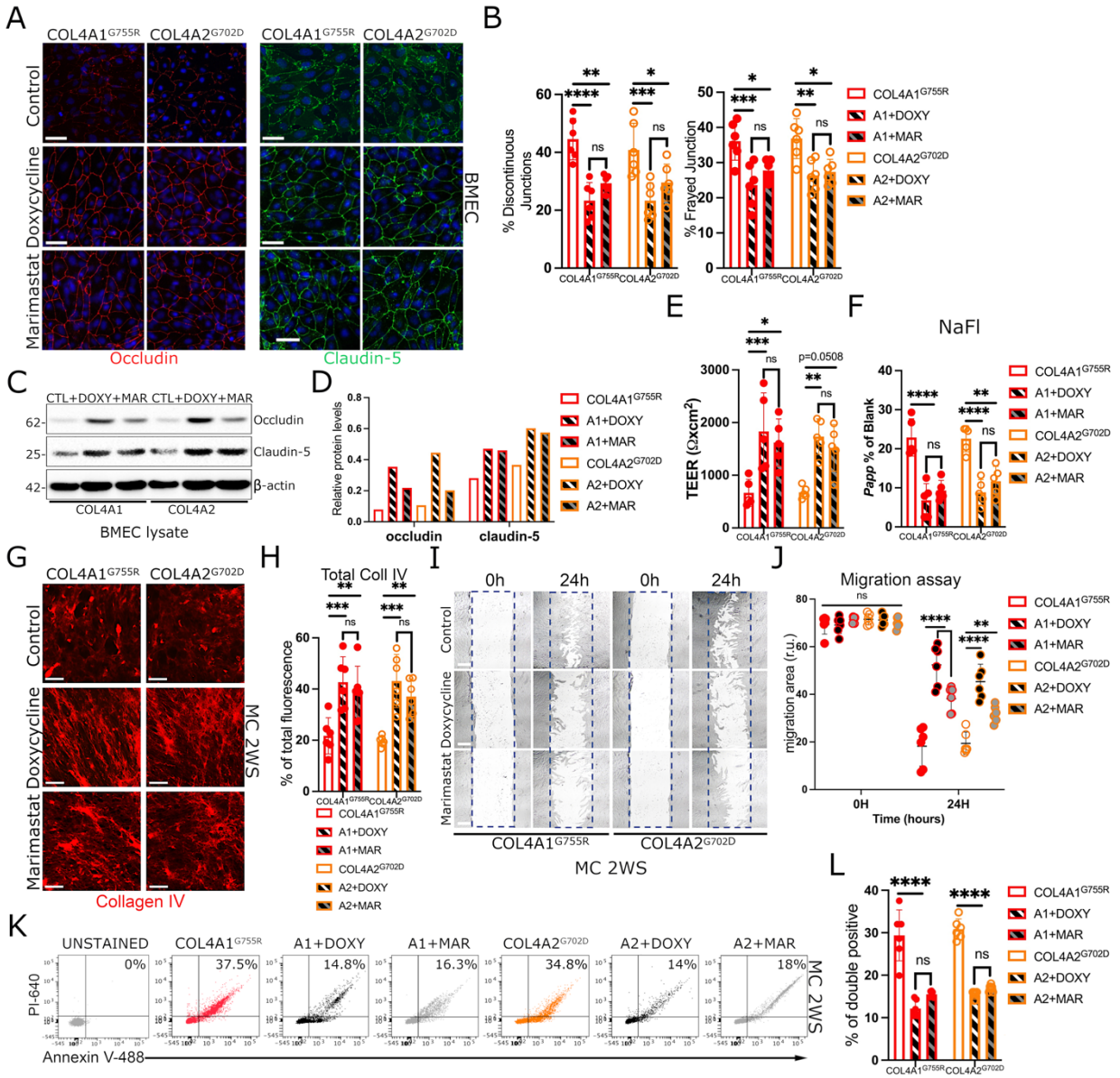

Figure 5. Doxycycline treatment ameliorates tight junction abnormalities and reverts COL4A1/A2 MC collagen IV defect and phenotypic changes.

A-B) Immunostaining analysis quantification of occludin and claudin-5 in COL4A1^{G755R} and COL4A2^{G702D} BMEC treated with doxycycline or marimastat for 4 days show lower percent of tight junction abnormalities (discontinuous and frayed junctions) compared to untreated control (DMSO) (n=6). **C-D)** Protein blot analysis and bands quantification show increased occludin and claudin-5 levels upon treatment with doxycycline (+DOXY) and marimastat (+MAR) (n=2). β-actin was used as loading control. Doxycycline and marimastat treatments improve both TEER **(E)** and NaF **(F)** readouts in *COL4A1/A2* mutant BMEC compared to untreated controls (n=6). **G)** Immunostaining analysis of collagen IV in the decellularized ECM of *COL4A1^{G755R}* and *COL4A2^{G702D}* MC at late stage (2WS) upon 4 days treatment with doxycycline (10uM) or marimastat (1uM), and total fluorescence quantification **(H)** show higher fluorescence in ECM compared to control (n=6). **I)** Representative image of scratch assay for *COL4A1/A2* hiPSC-derived MC control (DMSO), doxycycline treated and marimastat treated at 0 and 24 hours and scratch area quantification **(J)** show lower migration rate upon treatment with doxycycline or marimastat compared to controls (n=6). **K-L)** Doxycycline (+DOXY) and Marimastat (+MAR) treatments improve apoptotic levels in *COL4A1^{G755R}* and *COL4A2^{G702D}* MC 2WS compared to untreated (n=5). The results are presented as means ± SD of n independent

747 experiments *P<0.05; **P<0.01; ***P<0.001; ****P<0.0001; ns (not significant). Statistical
748 analysis was performed by 2-way ANOVA with Tukey's multiple comparison test.
749

Supplementary Figures

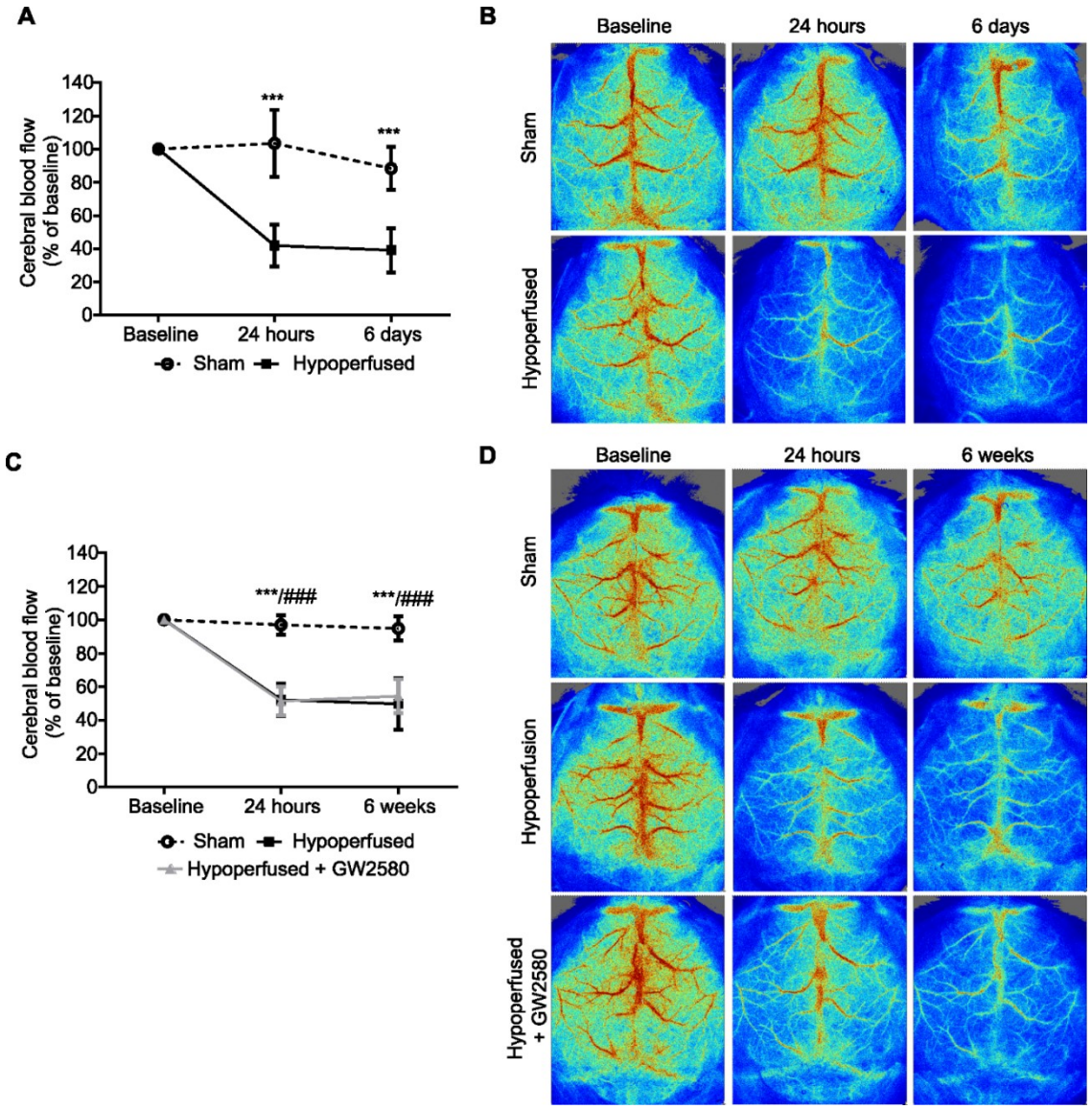

Supplementary Figure 1. Cortical cerebral blood flow is reduced post-BCAS. (A) BCAS surgery reduced CBF compared to sham at 24hr and 6 days. **(B)** Representative images of laser speckle flowmetry in sham and BCAS at baseline, 24 hours and 6 days.(**C**) BCAS surgery reduced CBF compared to sham at 24hr and 6 weeks and to a similar extent in the GW2580 treated group. **(D)** Representative images of laser speckle flowmetry in sham, BCAS vehicle and BCAS GW2580 animals at baseline, 24 hours and 6 weeks. Mean±SEM. ***p<0.001 (* indicates *post hoc* differences between sham and BCAS vehicle), $^{###}$p<0.001 ($^{#}$ indicates *post hoc* differences between sham and BCAS GW2580).

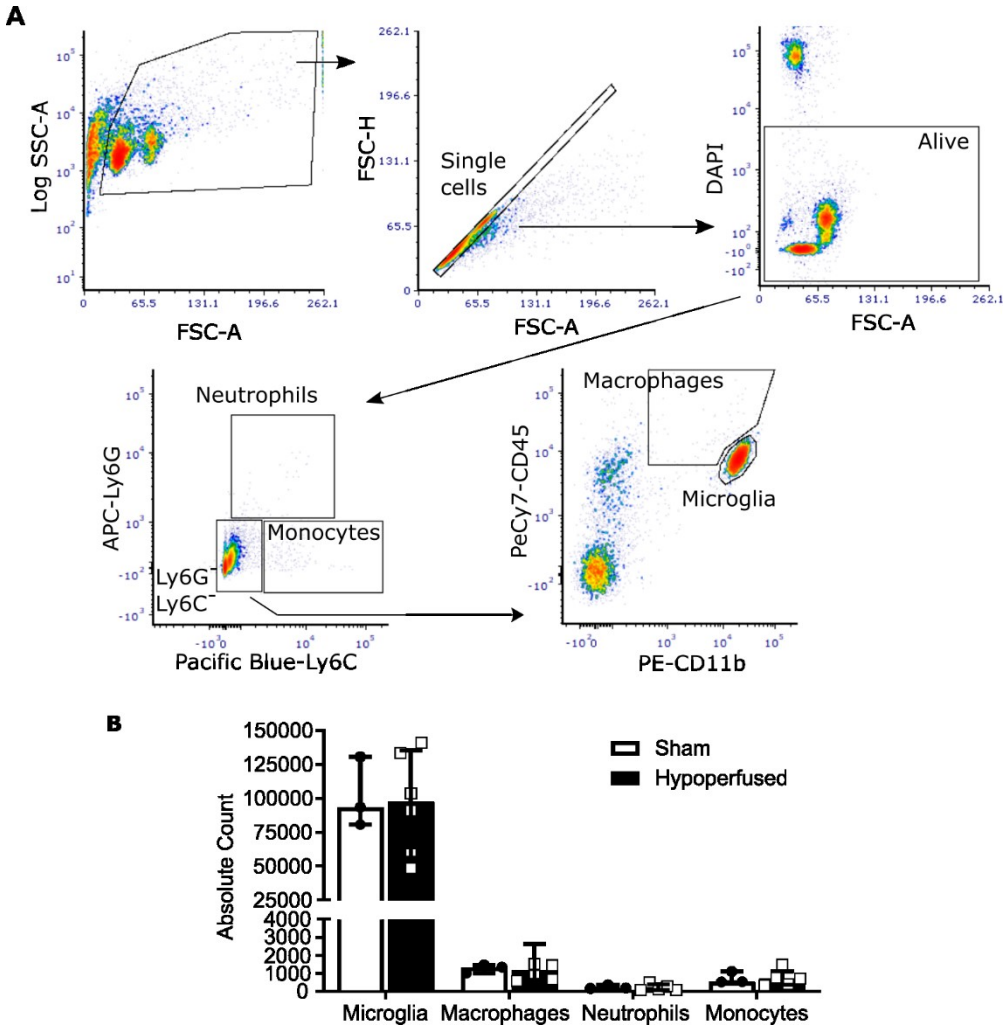

Supplementary Figure 2. **(A)** Full gating strategy and representative flow cytometry dot plots identifying neutrophil ($Ly6G^{+}$), monocyte ($Ly6C^{+}$), microglia ($CD11b^{+}$ $CD45^{low}$ $Ly6C^{-}$ Ly6G) and macrophage ($CD11b^{+}$ $CD45^{high}$ $Ly6C^{-}$ $Ly6G^{-}$) populations 7 days post-surgery. **(B)** Flow cytometric quantification of the absolute numbers of microglia, macrophages, neutrophils and monocytes in the grey matter of sham (n=3) and hypoperfused (n=6) mice, based on the gating strategy shown in **A**. There is no significant differences in these numbers between sham and hypoperfused mice.

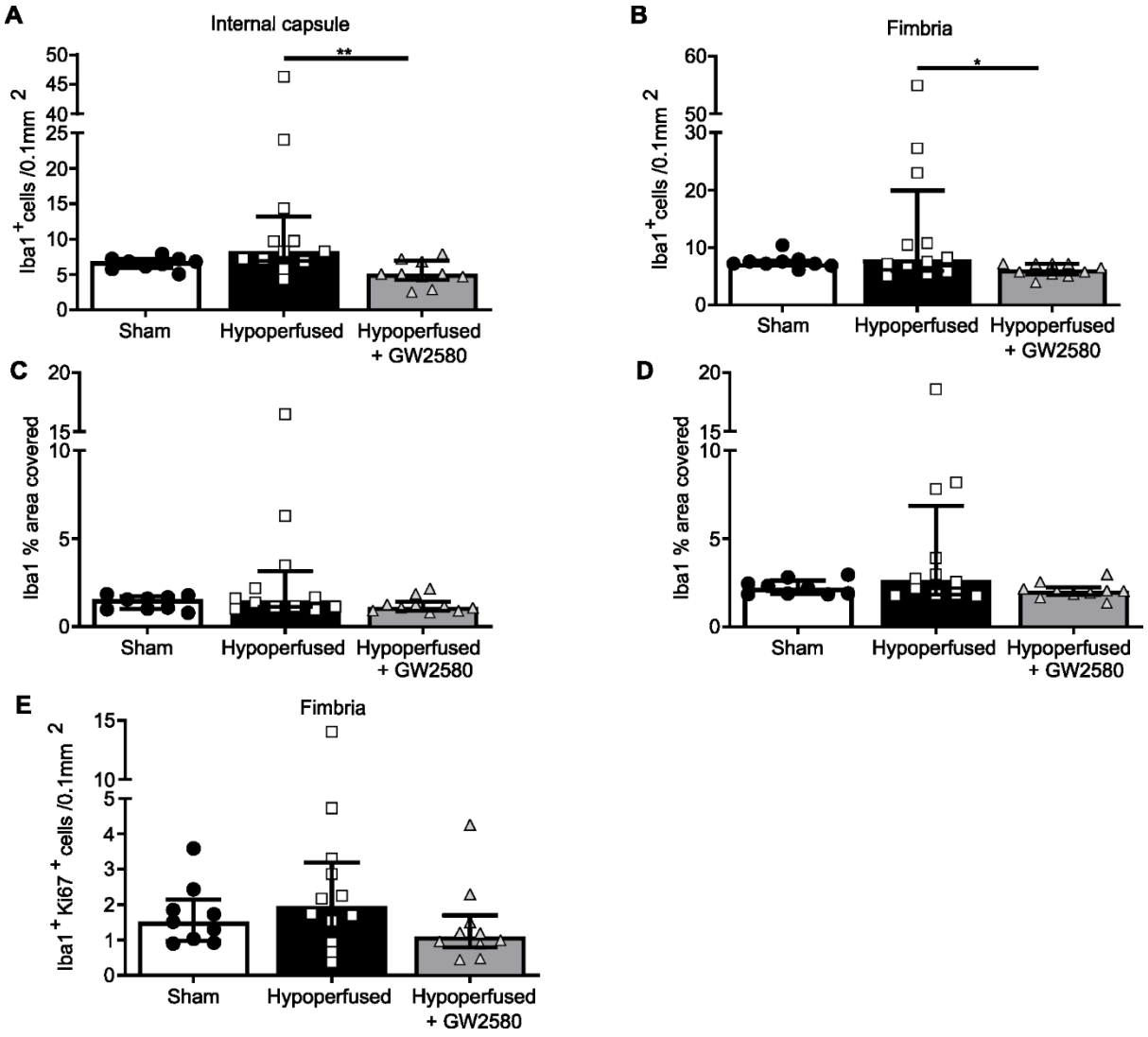

Supplementary Figure 3 CSF1R inhibition following chronic hypoperfusion prevents expansion of microglia in white matter regions. (A,B) Quantification of the number of microglial cells (Iba1^{+}) in the internal capsule (**A**) and fimbria (**B**); **(C,D)** Iba1% area staining as a measure of microglial activation in the in the internal capsule (**C**) and fimbria (**D**) following 6 weeks of hypoperfusion and GW2580 treatment. **(E)** Quantification of the number of proliferating microglial cells (Iba1^{+} Ki67^{+}) in the fimbria following chronic hypoperfusion and GW2580 treatment. Data presented as mean ± SD and analysed by one-way ANOVA with *post hoc* Bonferroni correction, *p<0.05, **p<0.01.

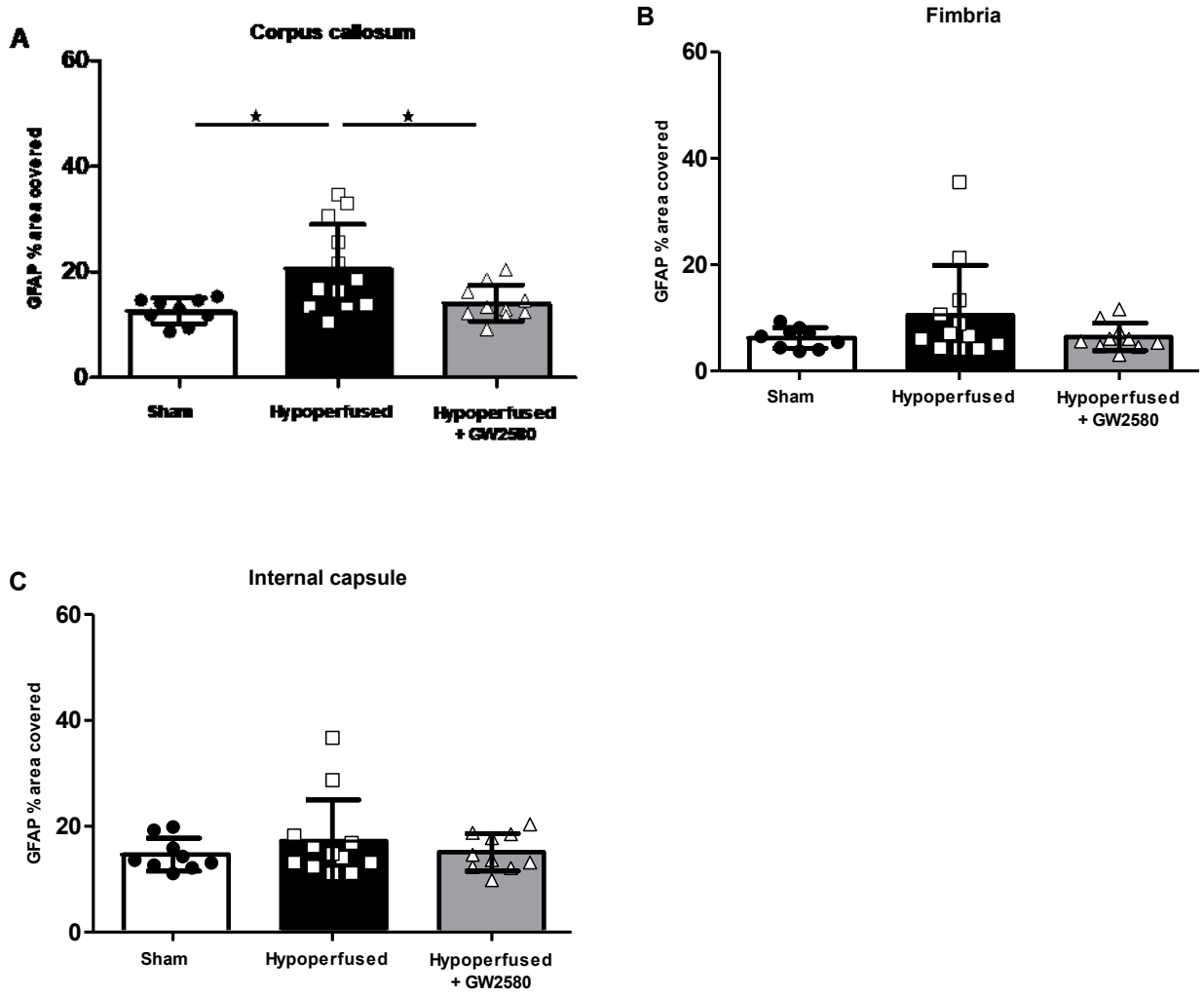

Supplementary Figure 4 CSF1R inhibition following chronic hypoperfusion modestly reduces astrogliosis in white matter regions. (A) Astrogliosis was increased in the hypoperfused vehicle group compared to shams and the hypoperfused GW2580 group in the corpus callosum. Astrogliosis was not significantly altered in the fimbria **(B)** and the internal capsule **(C)**. Data presented as mean ± SD and analysed by one-way ANOVA with *post hoc* Bonferroni correction, *p<0.05.

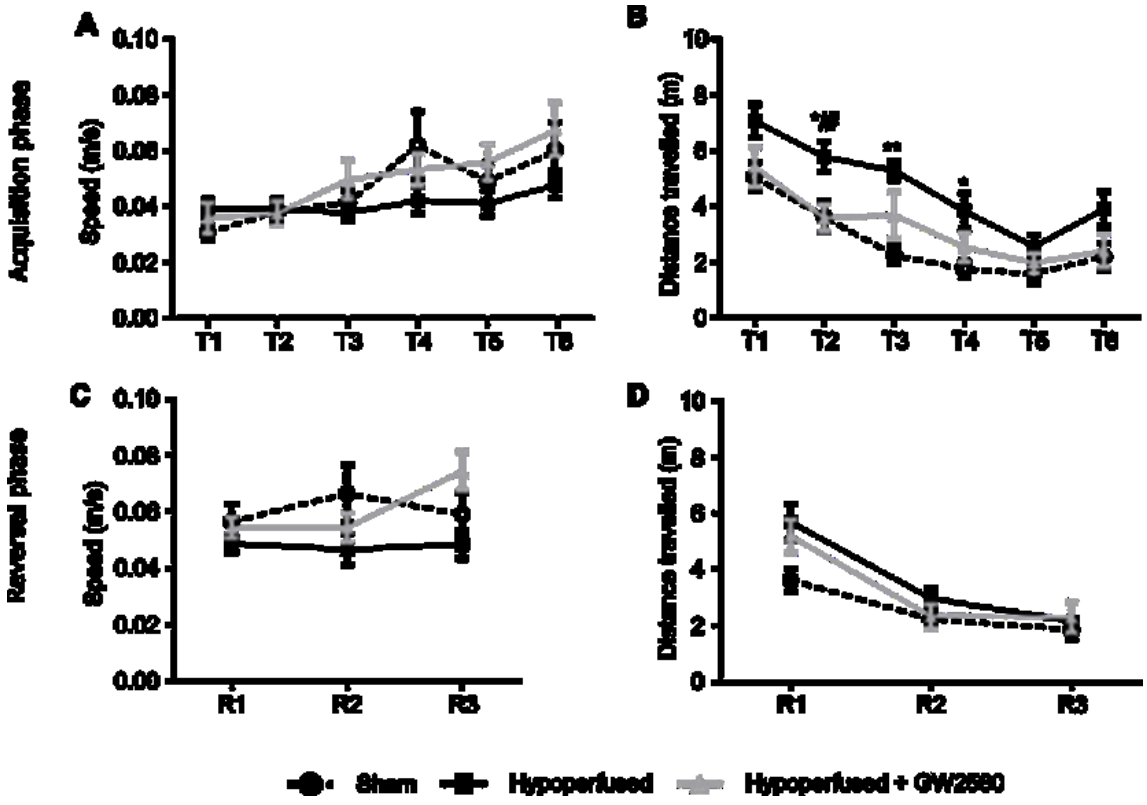

Supplementary Figure 5: Movement speed is unaffected by hypoperfusion or GW2580 treatment. (A) Quantification of movement speed (metres per second) across the 6 training days in the acquisition phase of the Barnes maze. Each training day represents an average of 2 trials. **(B)** Quantification of total distance travelled (m) across the 6 training days in the acquisition phase. **(C)** Quantification of movement speed (metres per second) across the 3 training days in the reversal phase of the Barnes maze. Each training day represents an average of 2 trials. **(D)** Quantification of total distance travelled (m) across the 3 training days in the reversal phase. Data presented as mean ± SEM and analysed by repeated measures two-way ANOVA with *post hoc* Bonferroni correction. *$p<0.05$, **$p<0.01$, $^{\#}p<0.05$, * sham vs. hypoperfused, # hypoperfused vs hypoperfused + GW2580.